Computers & Geosciences 63 (2014) 62–69

Contents lists available at ScienceDirect

Computers & Geosciences

journal homepage: www.elsevier.com/locate/cageo

A numerical model of ballistic transport with collisions in a volcanic setting

Kae Tsunematsu [a,c,*], Bastien Chopard [b], Jean-Luc Falcone [b], Costanza Bonadonna [c]

[a] Graduate School of Environmental Studies, Nagoya University, Nagoya, Japan
[b] Department of Computer Science, University of Geneva, Geneva, Switzerland
[c] Section of Earth and Environmental Sciences, University of Geneva, Geneva, Switzerland

ARTICLE INFO

Article history:
Received 1 July 2013
Received in revised form
19 October 2013
Accepted 23 October 2013
Available online 30 October 2013

Keywords:
Volcanic eruption
Ballistic transport
Discrete Event Simulation (DES)

ABSTRACT

Fragments associated with explosive volcanic eruptions range from microns to meters in diameter, with the largest ones following ballistic trajectories from the eruptive vent. Recent field observations suggest that bombs ejected during Strombolian eruptions may collide while airborne. We developed a Discrete Event Simulator to study numerically the impact of such collisions on hazard assessment. We show that the area where bombs can land might be significantly increased when collisions occur. As a consequence, if collisions are dominant, the deposition distance cannot be used to estimate important eruption parameters, such as exit speed.

1. Introduction

When a volcano erupts explosively, volcanic particles of various sizes and shapes are ejected from the vent. Large particles (>64 mm) are transported in the air, decoupled from the gas phase at the early stage of transport, and follow independent parabolic trajectories. These large particles are called ballistic blocks or bombs, or simply ballistics. Their study is crucial as the kinetic energy and high temperature associated with ballistics can significantly damage infrastructures in proximal areas. In addition, the behavior of bombs allows a better understanding of the dynamics of ejection because their velocity is more strongly related to the jet phase than to the convective phase of a volcanic plume.

There are many numerical models describing the trajectory of the individual particles. A numerical model of volcanic bombs was first suggested by Wilson (1972) which accounted for the effect of drag forces. It was further developed by Fagents and Wilson (1993) with realistic conditions including the coupling between the explosion and surrounded air for Vulcanian eruptions. Bower and Woods (1996) considered ballistic trajectories which were accelerated by the gas phase, while taking into account the particle motion through the crater and the atmosphere.

Alatorre-Ibargüengoitia and Delgado-Granados (2006) measured drag force of ballistic particles due to the shape difference in laboratory experiments. The effect of fragmentation on the initial velocity of ballistics in Vulcanian eruptions has been included. The results were applied to the hazard map of Popocatépetel volcano (Alatorre-Ibargüengoitia et al., 2012).

Mastin (2002) proposed a Graphical User Interface (GUI) with which researchers can investigate their own scenario. Saunderson (2008) suggested equations of motion with the resistance and total centrifugal terms by using plural particles. Recently, de'Michieli Vitturi et al. (2010) suggested a Lagrangian model of large volcanic particles subject to a drag force and the background flow field of the plume. However none of these models consider the effect of inter-particle collisions.

Recently Vanderkluysen et al. (2012) reported collisions between particles. Particle trajectories were extracted from thermal video images of Strombolian eruptions. According to these trajectories, 12% of the analyzed particles experienced a collision with another particle. This suggests that inter-particle collisions should be implemented in numerical models aimed at predicting the trajectories of bombs.

In this paper, we propose a numerical model that includes inter-particle collisions. We investigate their effect on pyroclast travel distances, which is directly related to hazard assessment. In order to highlight the role of collisions in the ballistic process, we neglect the drag force. This allows us to use a Discrete Event Simulation (DES) method, which is a fast numerical approach.

The parameters of our model are based on observations of Strombolian eruptions. In addition to the thermal video images

* Corresponding author at: Graduate School of Environmental Studies, Nagoya University, Nagoya, Japan.
E-mail address: kae.tsunematsu@gmail.com (K. Tsunematsu).

0098-3004/$ - see front matter
http://dx.doi.org/10.1016/j.cageo.2013.10.016

from Vanderkluysen et al. (2012), the initial velocity of particles, their ejection angles and the frequency of bursts can be extracted from the work of Chouet et al. (1974), Blackburn et al. (1976), Ripepe et al. (1993) and Patrick et al. (2007) where photos of short exposure time are analyzed to obtain the trajectory of particles. Ejection velocity, maximum height of particle during the flight and eruption durations can be obtained from Patrick et al. (2007) where thermal video (Forward Looking Infrared Radiometer) studies are reported.

In the present work, we consider a sensitivity analysis of the ballistic process with respect to collisions. We study which parameters affect most the probability of collision, and which parameters influence the travel distance of the bombs when collisions are taken into account. Our main result is that the area in which bombs are likely to fall may significantly increase when collisions occur.

2. The model

2.1. Initial parameters

Our numerical model simulates an eruption as a series of successive bursts. A burst is the simultaneous ejection of N_p spherical particles of radius R and density ρ_p. Bursts are events that are instantaneous and repeat every time interval Δt_b, as illustrated in Fig. 1. During a burst, N_p particles are ejected at once. The time of the first burst is defined as $t=0$. The time of the last burst is denoted T_l, an input parameter of the model. The number of bursts N_b is then given by $T_l/\Delta t_b$. The total number of particles N that are ejected during the full simulated eruption is therefore $N = N_b \times N_p$.

Each ejected particle is characterized by its offset position $\vec{r}_e$ with respect to the center of the vent, and its initial velocity $\vec{v}_e$.

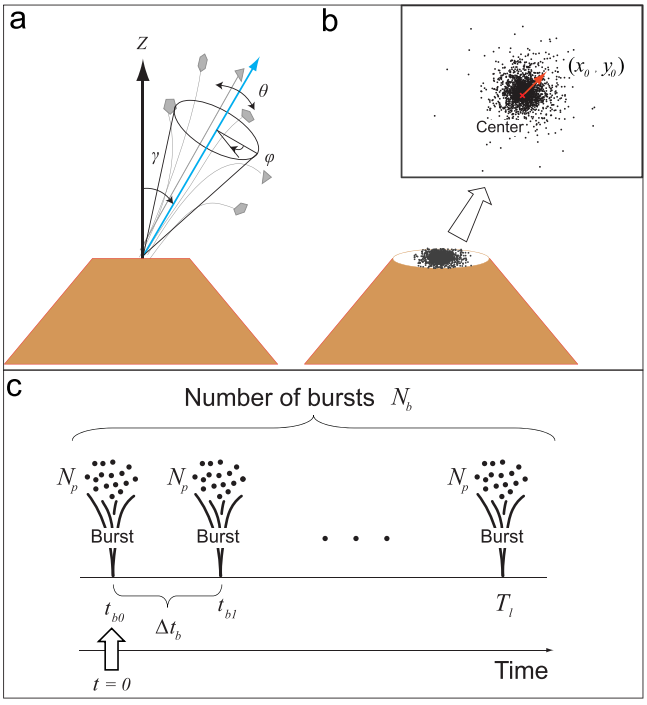

Fig. 1. Input parameters. (a) Rotation angle (γ), inclination angle (θ) and azimuth angle (ϕ). (b) Displacement of ejection point from the vent center $r_e = (x_0, y_0, 0)$. (c) Parameters related to bursts such as number of bursts (N_b) and number of particles per burst (N_p). Burst time interval Δt_b is the time between t_{b0} and t_{b1} ($\Delta t_b = t_{b1} - t_{b0}$). Time of last burst T_l is given deterministically and the number of bursts N_b is controlled by burst time interval Δt_b.

The ejection speed is defined by its magnitude v and its direction is given by three angles, γ (rotation), θ (inclination) and ϕ (azimuth), as shown in Fig. 1. The rotation angle γ accounts for the fact that the vent orientation, or the conduit shape, may depart from the vertical direction. Assuming that the x-axis is chosen so that the xz-plane contains the vector normal to the vent, the velocity vector $\vec{v}_e$ is obtained as

$$\vec{v}_e = \begin{pmatrix} \cos\gamma & 0 & \sin\gamma \\ 0 & 1 & 0 \\ -\sin\gamma & 0 & \cos\gamma \end{pmatrix} \begin{pmatrix} v\sin\theta\cos\phi \\ v\sin\theta\sin\phi \\ v\cos\theta \end{pmatrix} \tag{1}$$

The above parameters are summarized in Table 1. In our simulation, their value, for each event and each particle, is chosen from a probability distribution to reflect their uncertainty. The types of distributions are shown in Table 2 and have been determined from the observations reported in Vanderkluysen et al. (2012), Chouet et al. (1974), Blackburn et al. (1976) and Patrick et al. (2007).

2.2. Ballistic movement and collisions

Once a particle has been ejected from a given vent location, with a given initial velocity, it follows a parabolic trajectory $\vec{r}(t)$, due to gravity, until it reaches the ground or collides with another airborne particle. In the present study we disregard the effect of the drag force. One reason is to better highlight, in a simple situation, the role of collisions compared to the situation without collisions. Secondly, neglecting the drag force allows us to significantly speed up the simulations by using the DES approach discussed in Section 2.3. Computation speed is important as we need to perform a large number of simulations to sample the space of possibilities.

The landing position of a particle on the ground is obtained by solving the equation $G(\vec{r}(t)) = 0$, where $G(x,y,z) = 0$ is the relation describing the ground profile. If $G(x,y,z)$ is a simple function (e.g. $G(x,y,z) = z - z_0$ as we use here), the time of the impact and its location can be computed analytically.

To solve the collision process, we use standard classical mechanics. Let us denote by $\vec{r}_i(t)$ the trajectory of particle i, with radius R_i. The pair of particles (i, j) that will collide first is determined. This is the pair for which the solution of $|\vec{r}_i(t) - \vec{r}_j(t)| \le R_i + R_j$ yields the smallest time t which is not smaller than current time.

This time t can be computed analytically for any pair of parabolic trajectories. For instance, let us consider particles 1 and 2:

$$\begin{aligned} \vec{r}_1(t) &= \vec{r}_1^{(0)} + \vec{v}_1^{(0)}(t - t_1) + \tfrac{1}{2}\vec{g}(t - t_1)^2 \\ \vec{r}_2(t) &= \vec{r}_2^{(0)} + \vec{v}_2^{(0)}(t - t_2) + \tfrac{1}{2}\vec{g}(t - t_2)^2 \end{aligned} \tag{2}$$

where t_i is the time at which particle i is ejected from position $\vec{r}_i^{(0)}$ with velocity $\vec{v}_i^{(0)}$, and $\vec{g} = (0, 0, -9.81)$ is the gravity. It is then easy to show that $\vec{r}_1(t) - \vec{r}_2(t)$ is a linear function in time:

$$\vec{r}_1(t) - \vec{r}_2(t) = \vec{a} + \vec{b}\,t \tag{3}$$

with

$$\vec{a} = \vec{r}_1^{(0)} - \vec{r}_2^{(0)} - \vec{v}_1^{(0)} t_1 + \vec{v}_2^{(0)} t_2 + \tfrac{1}{2}\vec{g}(t_1^2 - t_2^2) \tag{4}$$

and

$$\vec{b} = \vec{v}_1^{(0)} - \vec{v}_2^{(0)} - \vec{g}(t_1 - t_2) \tag{5}$$

Table 1
Parameter notation, distributions and inputs. μ represents average and σ represents standard deviation. $\mathcal{N}(\mu,\sigma)$ indicates normal (=Gaussian) distribution defined by the mean μ and the standard deviation σ. Note that when a value out of range (e.g. $\rho_p<0$) is generated, it is re-drawn. $\mathcal{U}$(min, max) indicates uniform distribution between the minimum min and the maximum max.

Parameter	Notation	Distribution	Input
Particle density (kg/m^3)	ρ_p	$\rho_p=\mathcal{N}(\mu_{\rho p},\sigma^2_{\rho p})$	$\mu_{\rho p}$, $\sigma_{\rho p}$
Particle diameter (m)	$D=2R$	$D=\mathcal{N}(\mu_D,\sigma^2_D)$	μ_D, σ_D
Magnitude of initial velocity (m/s)	$v=\lvert\vec{v}_e\rvert$	$v=\mathcal{N}(\mu_v,\sigma^2_v)$	μ_v, σ_v
Rotation angle (deg., **rotation from vertical axis**)	γ	*Deterministic* $\gamma\in\left[0,\frac{\pi}{2}\right]$	γ
Inclination angle (deg.), **from vertical axis**)	θ	$\theta=\mathcal{N}(0,\sigma_\theta)$	σ_θ
Azimuth angle (deg.)	ϕ	$\phi=\mathcal{U}(0,2\pi)$	–
Displacement of ejection points from the vent center (m)	$\vec{r}_e=\begin{pmatrix}x_0\\y_0\\0\end{pmatrix}$	$x_0=\mathcal{N}(0,\sigma_r^2)$ $y_0=\mathcal{N}(0,\sigma_r^2)$	σ_r
Number of particles per burst	N_p	$N_p=\mathcal{N}(\mu_{N_p},\sigma^2_{N_p})$	μ_{N_p}, σ_{N_p}
Number of bursts	N_b	$N_b=T_l/\Delta t_b$	–
Total number of particles	N	$N=N_p\times N_b$	–
Burst time interval (s)	Δt_b	$\Delta t_b=\mathcal{N}(\mu_{\Delta t_b},\sigma^2_{\Delta t_b})$	$\mu_{\Delta t_b}$, $\sigma_{\Delta t_b}$
Time of last burst (s)	T_l	*Deterministic* $T_l\in[0,\infty]$	T_l

Table 2
Values of input parameters for our analysis (from Vanderkluysen et al., 2012; Chouet et al., 1974; Blackburn et al., 1976; Patrick et al., 2007).

Parameter	Unit	Input	Value
Particle density	kg/m^3	$\mu_{\rho p}$	1450
		$\sigma_{\rho p}$	500
Particle diameter	m	μ_D	0.5
		σ_D	0.3
Magnitude of initial velocity	m/s	μ_v	40
		σ_v	10
Standard deviation of inclination angle	deg.	σ_θ	5
Rotation angle	deg.	γ	0
Displacement of ejection points from the vent center	m	σ_r	10
Number of particles per burst		μ_{N_p}	20
		σ_{N_p}	0
Burst time interval	s	$\mu_{\Delta t_b}$	0.1
		$\sigma_{\Delta t_b}$	0
Time of last burst	s	T_l	10

As a result, the condition $\left(\vec{r}_1(t)-\vec{r}_2(t)\right)^2=(R_1+R_2)^2$ becomes the quadratic equation:

$$\vec{a}^2-(R_1+R_2)^2+2\vec{a}\cdot\vec{b}\,t+\vec{b}^2t^2=0 \tag{6}$$

which is easily solved analytically.

Note that since we do not discretize the time variable t, the probability to have a triple collision, or several simultaneous pair collisions, can be neglected.

The collision between the two selected particles is supposed to be instantaneous. Conservation of momentum, combined with the fraction of energy lost in the collision (given by the restitution coefficient C_R), is needed to compute the new velocity of the two particles after collision.

Let us call $\vec{v}_1$ and $\vec{v}_2$ the pre-collision velocities of the two particles. It is then well known (Landau and Lifshitz, 1976) that the problem can be solved by projecting the velocities on the unit vector $\vec{e}$ connecting the center of the two particles and the perpendicular direction. It can be shown that the following relations defines the post-collision velocities $\vec{v'}_1$ and $\vec{v'}_2$:

$$\vec{v'}_1=V'_1\vec{e}+\vec{v}_1-(\vec{v}_1\cdot\vec{e})\vec{e}$$
$$\vec{v'}_2=V'_2\vec{e}+\vec{v}_2-(\vec{v}_2\cdot\vec{e})\vec{e} \tag{7}$$

with

$$V'_1=\frac{(1+C_R)(-\vec{v}_1\cdot\vec{e}+\vec{v}_2\cdot\vec{e})}{m_1/m_2+1}+\vec{v}_1\cdot\vec{e}$$
$$V'_2=\frac{(1+C_R)(-\vec{v}_2\cdot\vec{e}+\vec{v}_1\cdot\vec{e})}{m_2/m_1+1}+\vec{v}_2\cdot\vec{e} \tag{8}$$

2.3. Discrete Event Simulation method

The above model can be efficiently implemented using a DES method (Banks and Nelson, 2010). The DES approach is very commonly used in the modeling and simulation of systems characterized by events that occur at well defined moment in time. Once such an event has occurred, the time of the next one can be computed precisely from the knowledge of the current situation.

Technically, a DES simulator consists of a “state” and a “queue of future events”. A state consists of the current simulation time t and the values of the variables describing the system at this time.

Events in the queue are processed until the queue becomes empty. When an event is processed, all states are updated and the events in the queue are modified by removing existing events or creating and inserting new events. Simulation time jumps from the time of one event to the time of next event. The list of events in the queue is always kept sorted by increasing time of occurrence, so that the next event to be processed is the first in the queue.

In our ballistic model, the state of the system is composed of (1) the current time, (2) the list of airborne particles, and (3) the list of deposited particles. Within these lists, each particle includes its density, diameter, position and velocity.

There are three types of events in our model: Burst (ejection of N_p particles), Collision and Deposition. Between events, trajectories are calculated analytically and new collision and deposition events can be obtained.

At the initialization, the event queue is filled with exogenous events, i.e. events which are caused by the external effects (here the burst). On the contrary, events which are caused by the internal evolution of the system are called endogenous events (here the collision and deposition).

At the beginning of the simulation all the particle ejections (burst events) are inserted in the event queue. Then all the collision and deposition times are computed according to the analytical formulas. All these events are added to the event queue while preserving the time ordering.

When a deposition takes place, the particle is moved from the airborne list to the deposition list, with the proper time and location of the event. The event is discarded from the list. The simulation jumps to the next event.

When collisions take place, the position and velocities of the two colliding particles are modified according to the momentum conservation law and the value of the restitution coefficient. Based on these new velocities, the collision and deposition events involving the two particles are updated. This means discarding the collisions which were planned if these two particles had not collided, and adding new collisions that may occur between these two particles and all the others.

3. Results and discussion

3.1. Impact of collision on the deposition area

Our model can simulate ballistic transport with or without collisions. Fig. 2(a) shows an example where collisions are ignored, even if particles get close enough. Fig. 2(b) shows a similar situation where collisions are enabled. We can observe that, with collisions, the traveled distance of the particles is increased.

This is confirmed by Fig. 3 which shows the spatial distribution of the deposited particles on a flat ground profile. The black circles divide the area around the crater into two regions where 75% and 99% of the particles have landed when collisions are enabled (red triangle). Green squares correspond to the ground deposition of the particles when collisions are disabled. The parameters of this simulation are those in Table 2, except for the particle diameter which is fixed to 1 m and the total number of particles is $N=2000$.

A typical scenario that explains the increase of the traveled distance is shown in Fig. 4. A small particle from a previous burst is falling back to the ground when it is hit by a larger particle just ejected during a more recent burst. As a result, the small particle is strongly deviated from its initial trajectory. Similar situations may also occur between particles of the same mass, as is the case in Fig. 3, but yet with a lesser effect than shown in Fig. 4.

3.2. Parameter study

The distribution of impacts on the ground when collisions are allowed depends on the parameters of the simulation. In this section we investigate the reasons that make particles fly farther away when collisions occur. We consider simulations with the parameters given in Table 2, except for the parameter whose importance is investigated.

Total number of particles: The role of the total number N of particles is considered in Fig. 5. To modify N, the number of bursts is increased but N_p, the number of particles per burst, is still given by the normal distribution of mean μ_{N_p} and standard deviation σ_{N_p}. Fig. 5 shows, for each value of N, the distance to the crater where a given percentage of the particle has been deposited. The cases with and without collisions are indicated. In the latter case, the spatial distribution of the particle is independent of N as expected.

As already noticed, when collisions are allowed, the spatial distribution of the ballistic impacts is expanded. A reason is that the total number of collision increases with N and the traveled distance tends to increase with the total number of collisions. However, this is not so simple and we will see below that a particle experiencing too many collisions does not travel very far. What is important to enlarge the deposition area is to have many particles that experience only one or two collisions while airborne.

Burst time interval: The deposition distance of the collision-allowed case is sensitive to the time interval between bursts. This

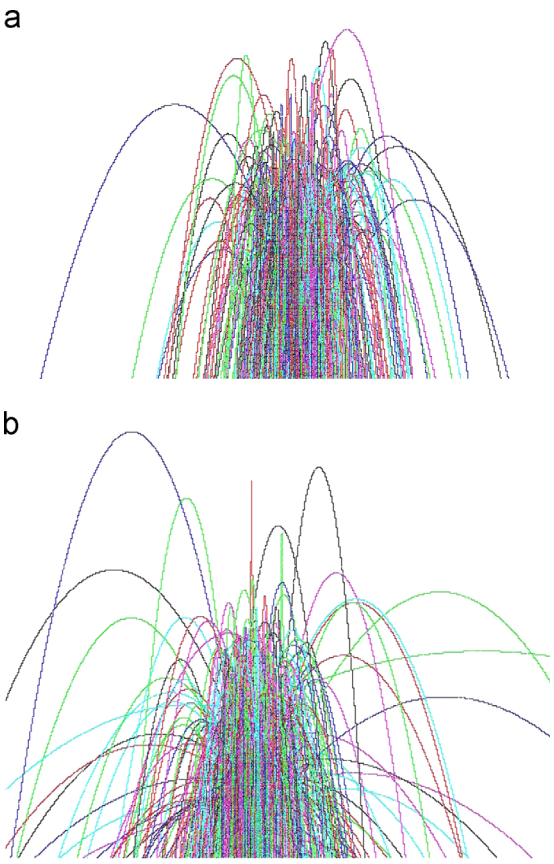

Fig. 2. Illustrations of the ballistic trajectories of 1000 particles for (a) an eruption without collisions and (b) an eruption with collisions. Different particles are shown with different colors. (For interpretation of the references to color in this figure caption, the reader is referred to the web version of this paper.)

dependency is absent when collision is disregarded. Fig. 6 (a) indicates the spatial distribution of the deposits. For short time interval Δt_b, the total number of collisions is important, as shown in Fig. 6(b), thus explaining the increase of the deposition range.

If Δt_b is increased to about 10 s, the deposition distances observed with and without collisions become almost the same. The number of inter-burst collisions also goes to zero for such values of Δt_b. This suggests that the important events to increase the travel distance are the collisions between particles ejected with a time lag, as in the scenario of Fig. 4.

It is easy to explain why, for time intervals larger than 10 s, the inter-burst collisions disappear. In our simulation we choose the average ejection speed to be $v_e = 40$ m/s. Thus, the expected deposition time t_d of a particle with such an initial velocity is $t_d = 2v_e/g = 8.15$ s, where g is the gravity acceleration. Therefore, if bursts are separated by about 10 s, almost all particles will have landed before the next burst.

In Ripepe et al. (1993) the change of mass flux as a function of time is reported for a Strombolian eruption. If the frequency of the change of mass flux is interpreted as the frequency of the bursts, the burst time interval of ballistics in the 1985–1986 Stromboli eruption is around 0.5–2.0 s. This is clearly shorter than the travel time of a particle ejected with an initial velocity of 40 m/s. Therefore, it is possible to have collisions between particles in successive bursts of a Strombolian eruption.

Additionally, Vanderkluysen et al. (2012) reported that 12% of particles experienced inter-particle collisions in Stromboli 2008 eruption. It means that bursts occurred from 0.5 to 1.0 s of time interval according to the results shown in Fig. 6(b). This number agrees with Ripepe et al. (1993) as discussed above.

Particle size: The effect of particle size on the total number of collisions and travel distance is demonstrated in Fig. 7. The number of collisions increases monotonically with the particle diameter (see Fig. 7(a)). As the particle size increases, the travel distance increases until a diameter of 150 cm. Then, the travel distance decreases (see Fig. 7(b)). We suggest that as the particle diameter increases, the number of collisions each particle experiences increases. As shown below, this is a factor limiting the traveled distance.

Restitution coefficient: The restitution coefficient C_R is a parameter that changes the velocity after the collision due to the energy lost when $C_R < 1$. Its value is difficult to estimate from field work. For this reason, we study all possible values of C_R from $C_R=0$ (totally inelastic collision) to $C_R=1$ (totally elastic collision). According to the travel distances shown in Fig. 8 for various restitution coefficients, one observes that particles travel farther in the collision-enabled case than in collision-disabled case, even when the restitution coefficient goes to zero. The travel distance is observed to increase almost linearly with C_R.

Relation between collisions and travel distance: As a general rule, we have observed that a particle which travels far collides only a few times before landing. Note that the total number of collisions (M) and the average number of collisions per particle (m) have to be distinguished. The relation between them is typically as follows: with a small total number of collisions M, one has a small number of particles that experience only one collision, thus $m < 1$. As M increases, more particles will experience one collision ($m \to 1$), up to the point where many particles experience many collisions ($m > 2$). That is why we argue that the deposition area first increases with M, and then decreases.

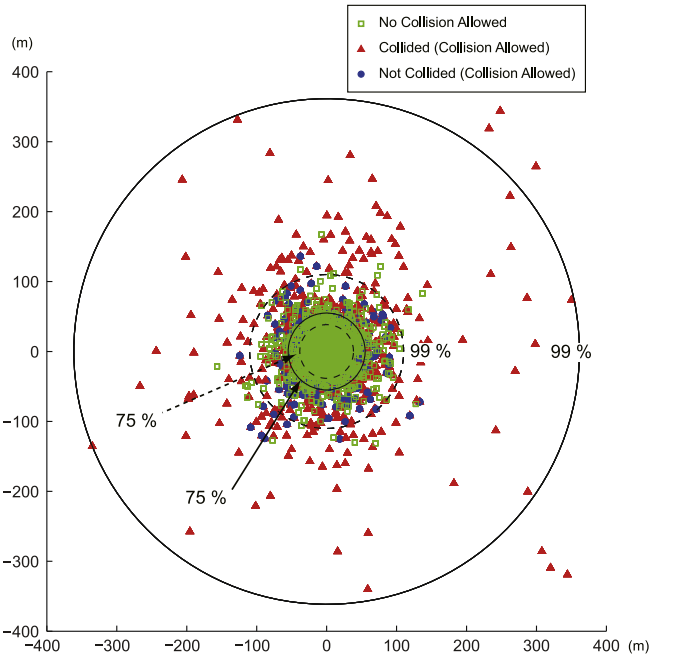

Fig. 3. Particle distribution on the ground (particle diameter = 1 m, 2000 particles). Symbols correspond to the deposition of single particles. Green squares indicate particle deposition when collisions are ignored. Blue circles indicate deposition for particles which did not collide even when collisions are allowed. Red triangles indicate deposition of particles having experienced a collision. Contours indicate the percentage of deposited particles within the contour: solid lines correspond to the case where collisions are allowed, and dashed lines for the case where collisions are ignored.

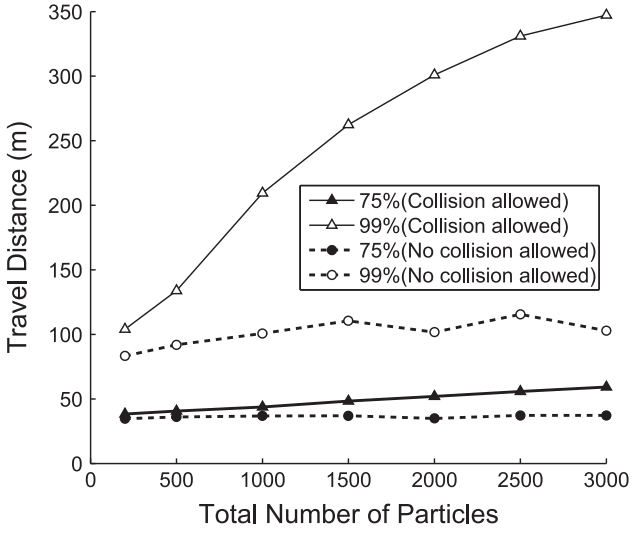

Fig. 5. Changes in the distribution of the deposition distance as a function of the total number N of particles ejected by the volcano. Cases with and without collision are shown.

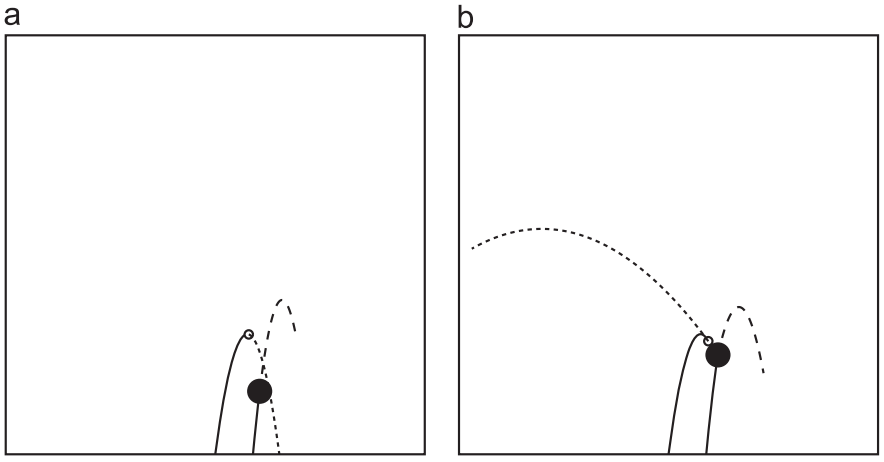

Fig. 4. Illustration of the trajectories of a two-particle collision. The light particle (white circle) has a mass of 3 kg, and is ejected at time $t_1 = 0$ with speed 56 m/s. The heavy one (black disk) has a mass of 81 kg and is ejected at time $t_2 = 4.8$ s, with speed 68 m/s. Panel (a) shows the trajectories before collision (solid lines) and the trajectories that would be followed if collision is ignored (dashed lines). Panel (b) shows the positions of the particles at the moment of the collision, at time $t = 7.6$ s. The dashed lines show their trajectories after collision. Just before collision, the light particle has a velocity of 16.6 m/s and the heavy one a velocity of 41.1 m/s. After collision, the speed of the light particle is 72.2 m/s and the speed of the heavy one is 38.7 m/s.

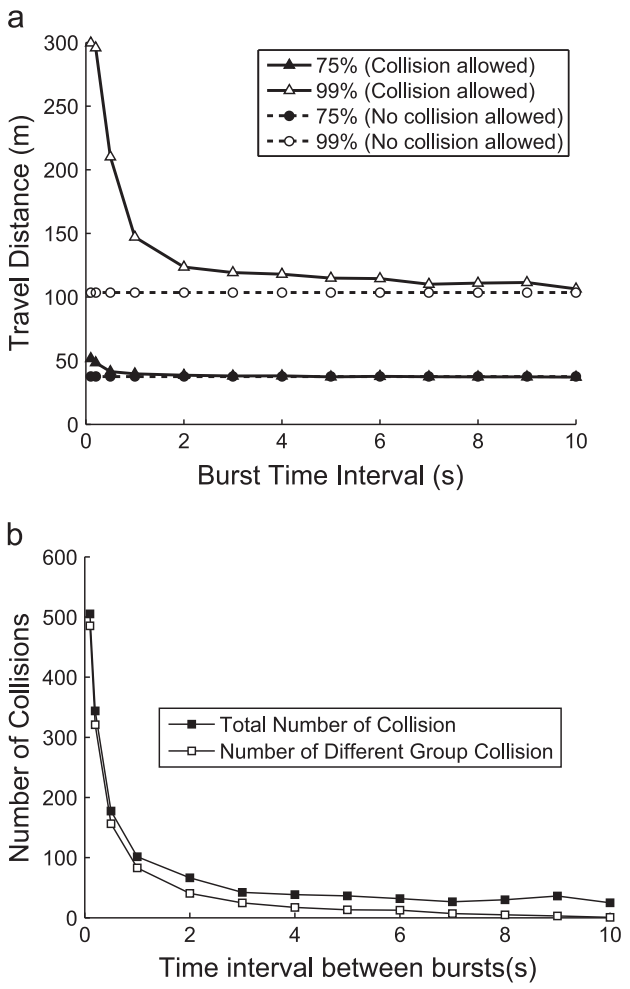

Fig. 6. (a) Deposition distance versus burst time interval. (b) Number of different group collisions versus burst time interval.

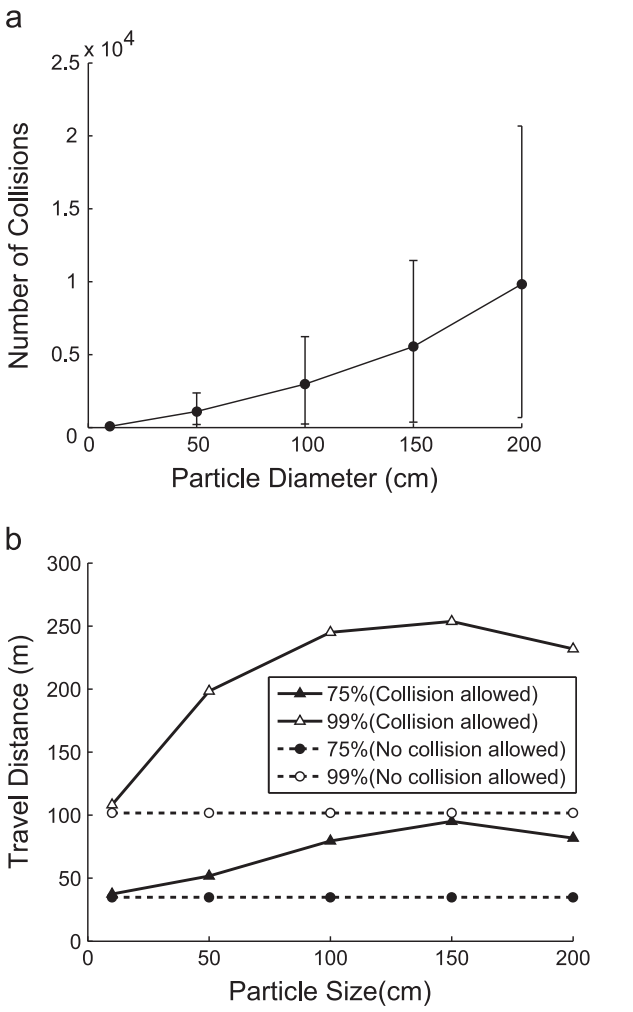

Fig. 7. (a) Number of collisions versus particle diameter. (b) Changes in deposition distance of collision-allowed cases and no-collision-allowed cases as a function of the particle diameter.

Our study also shows that a collision between a large and a small particle is likely to increase the deposition distance of the small particle. Accordingly, we have analyzed the relationship between the number of collisions that a single particle experiences and its deposition distance. We have also studied this relationship as a function of the particle mass.

As shown in Fig. 9(a) the deposition distance decreases as a given particle is subject to an increasing number of collisions. The most favorable event to travel far is to experience one or two collisions. Particles that collide more than 10 times do not go farther than 200 m. Particles that deposit farther than 500 m typically experienced less than 6 collisions.

The relationship between particle mass and deposition distance for each particle is shown in Fig. 9(b). The deposition distance decreases as the particle mass increases. The particle that traveled the farthest has collided only once and has a mass 1.9 kg. Its travel distance is 1900 m. In addition, we observe that the particles which travel more than 500 m have a mass smaller than 50 kg. Particles with a mass larger than 500 kg typically stay within 100 m of the vent. This supports the interpretation that light particles travel farther by receiving the large momentum from the heavy ones.

Without collisions, and provided that all particles are ejected from the crater with the same speed, the mass distribution in the landing area would be uniform. Therefore, if a non-uniform spatial distribution of the mass of particles is observed around the crater, as in Fig. 9(b), this could be a sign of the occurrence of airborne collisions.

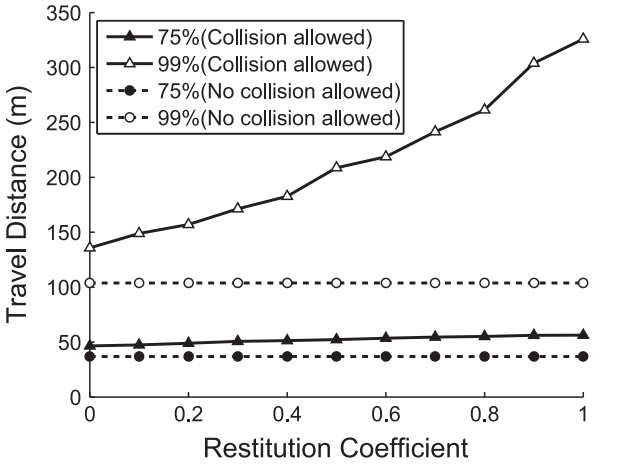

Fig. 8. Changes in deposition distance for the cases with and without collisions as a function of the restitution coefficient.

Note that some papers (e.g. Rosi et al., 2006; Wright et al., 2007) proposed to estimate the velocities of ballistics from the deposition distance. If collisions may occur during the flight in the air, such a calculation can no longer be considered. Direct measurement of the ejection speed is therefore recommended unless one can exclude the presence of collisions.

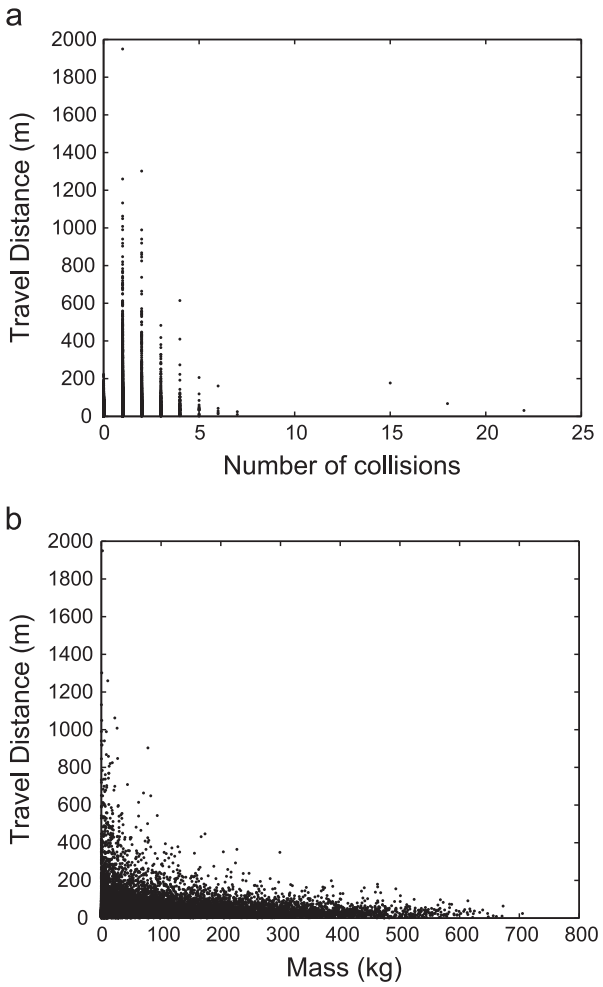

Fig. 9. (a) Deposition distance versus the number of collisions experienced by each particle during a simulation. (b) Deposition distance versus the mass of each particle. The results of ten simulation runs are merged in the plot.

3.3. Collision effect versus drag effect

Although we neglected the drag force in this study, some comments can be made. By using the same simulation conditions as before (see Table 2), we have computed that the travel distance of a particle subject to a drag force is reduced by about 20–50%, depending on its size. On the other hand, the present study (Figs. 5–8) demonstrated that collisions extend the travel distances by a factor of two to six. From these figures, we can conclude that collisions have a larger potential to modify the travel distance than the drag force. When both collisions and drag affect the trajectories of the particles, we can argue that collisions will increase the travel distance with respect to the situation where only the drag force is present. However, this distance cannot be quantified without performing detailed simulations. This will be considered in a forthcoming paper.

3.4. Applicability of the model to various types of eruption

As discussed in Section 3.2, the most relevant parameter that governs the collision rate is the time interval between bursts. Consequently, Strombolian eruptions are the most likely explosive events to be subject to inter-particle collisions. However, it is expected that Strombolian fragments may experience a significant drag force due to their vesicular nature, in which case, our model would overestimate the actual travel distance. Recently, it has been observed that also Vulcanian/subplinian eruptions can experience pulsating activity at vent. As an example, Ripepe et al. (2013) have shown how the eruptive plume generated during the Eyjafjallajökull 2010 eruption (Iceland) was characterized by discrete pulses injected into the atmosphere every 20 s for 5–6 s each. Pulsating eruptive behavior at source has already been observed during other volcanic eruptions of various magma compositions (e.g. Ruapehu, Bonadonna et al., 2005; Cerro Negro, Hill et al., 1998; Etna, Vergniolle and Ripepe, 2008; Andronico et al., 2008). However, it is expected that Strombolian particles may experience a significant drag force due to their vesicular nature. Therefore, our model may well overestimate the actual travel distance.

4. Conclusions

We have implemented three-dimensional ballistic simulations taking into account the collisions between particles. As much as possible, the parameters of the model are taken from field observations reported in the literature for Strombolian eruptions at Stromboli volcano.

From this model, the particle distribution on the ground can be computed and hazard maps, which accounts for inter-particles collisions, can be produced.

To our knowledge, this is the first study which investigates the effect of collisions on the size of the deposition area around the crater and performs a sensitivity analysis. As we assume parabolic trajectories for the bombs, we can compute analytically the collision events and efficiently implement our model with a DES method.

From our analysis of the simulation results, we conclude that

1. The collision probability is mostly affected by the burst time interval. The most efficient collisions happen between particles ejected in different bursts.
2. Effects of inter-particle collisions is most important for explosive volcanic eruptions characterized by pulsating behavior at source (e.g. Strombolian, violent Strombolian, long-lasting Vulcanian eruptions).
3. The travel distance of the particles increases with the total number of collisions up to the point where individual particles experience more than a few of them. Too many collisions per particles have a neutralizing effects.
4. The mechanism that makes a particle travel farther when it experiences a collision is the transfer of momentum that occurs during the impact. The favorable events are those where the speeds of the colliding particles form an angle close to 180°. The effect is enhanced when the mass of the particle going up is larger than the mass of the particle going down.
5. The spatial distribution of the mass of deposited particles is affected by the presence of collisions. This distribution can then be studied to assess the existence of collision during the eruption. As a consequence, if collision is dominant, the deposition distance cannot be used to derive important eruption parameters, such as the exit speed.
6. The increase of the travel distance is visible for any value of the restitution coefficient. However, the increase is more pronounced when the kinetic energy is conserved ($C_R=1$).
7. The effect of collisions on the travel distance of the particles is as significant in magnitude as the drag effect, but in an opposite direction.

References

Alatorre-Ibargüengoitia, M.A., Delgado-Granados, H., 2006. Experimental determination of drag coefficient for volcanic materials: calibration and application of a

model to Popocatépetl volcano (Mexico) ballistic projectiles. Geophys. Res. Lett. 33 5 pp.
Alatorre-Ibargüengoitia, M.A., Delgado-Granados, H., Dingwell, D.B., 2012. Hazard map for volcanic ballistic impacts at Popocatépetl volcano (Mexico). Earth Planet. Sci. Lett. 74, 2155–2169.
Andronico, D., Scollo, S., Caruso, S., Cristaldi, A., 2008. The 2002–03 Etna explosive activity: Tephra dispersal and features of the deposits. J. Geophys. Res. 113.
Banks, J., Nelson, B., 2010. Discrete-Event System Simulation. Prentice Hall.
Blackburn, E., Wilson, L., Sparks, R., 1976. Mechanisms and dynamics of strombolian activity. J. Geol. Soc. Lond. 132, 429–440.
Bonadonna, C., Phillips, J., Houghton, B.F., 2005. Modeling Tephra sedimentation from a Ruapehu weak plume eruption. J. Geophys. Res. 110, 1–22.
Bower, S.M., Woods, A.W., 1996. On the dispersal of clasts from volcanic craters during small explosive eruptions. J. Volcanol. Geotherm. Res. 73, 19–32.
Chouet, B., Hamisevicz, N., Mcgetchin, T.R., 1974. Photoballistics of volcanic jet activity at Stromboll, Italy. J. Geophys. Res. 79, 4961–4976.
de' Michieli Vitturi, M., Neri, A., Ongaro, T.E., Savio, S.L., Boschi, E., 2010. Lagrangian modeling of large volcanic particles: application to vulcanian explosions. J. Geophys. Res. 115.
Fagents, S., Wilson, L., 1993. Explosive volcanic eruptions: VII. the ranges of pyroclasts ejected in transient volcanic explosions. Geophys. J. Int. 113, 359–370.
Hill, B.E., Connor, C.B., Jarzemba, M.S., La Femina, P.C., Navarro, M., Strauch, W., 1998. 1995 Eruptions of Cerro Negro volcano, Nicaragua, and risk assessment for future eruptions. Geol. Soc. Am. Bull. 110, 1231–1241.
Landau, L., Lifshitz, E., 1976. Mechanics 1. Course of Theoretical Physics. Elsevier Butterworth-Heinemann.
Mastin, L.G., 2002. A Simple Calculator of Ballistic Trajectories for Blocks Ejected During Volcanic Eruptions. U.S. Geological Survey Open-File Report 01-45, Version 1.1. U.S. Department of the Interior, U.S. Geological Survey.
Patrick, M.R., Harris, A.J.L., Ripepe, M., Dehn, J., Rothery, D.A., Calvari, S., 2007. Strombolian explosive styles and source conditions: insights from thermal (FLIR) video. Bull. Volcanol. 69, 769–784.
Ripepe, M., Rossi, M., Saccorotti, G., 1993. Image processing of explosive activity at Stromboli. J. Volcanol. Geotherm. Res. 54, 335–351.
Ripepe, M., Bonadonna, C., Folch, A., Donne, D.D., Lacanna, G., Marchetti, E., Hskuldsson, A., 2013. Ash-plume dynamics and eruption source parameters by infrasound and thermal imagery: the 2010 Eyjafjallajkull eruption. Earth Planet. Sci. Lett. 366, 112–121.
Rosi, M., Bertagnini, A., Harris, A.J.L., Pioli, L., Pistolesi, M., Ripepe, M., 2006. A case history of paroxysmal explosion at Stromboli: timing and dynamics of the April 5, 2003 event. Earth Planet. Sci. Lett. 243, 594–606.
Saunderson, H.C., 2008. Equations of motion and ballistic paths of volcanic ejecta. Comput. Geosci. 34, 802–814.
Vanderkluysen, L., Harris, A.J.L., Kelfoun, K., Bonadonna, C., Ripepe, M., 2012. Bombs behaving badly: unexpected trajectories and cooling of volcanic projectiles. Bullet. Volcanol. 74 (8), http://dx.doi.org/10.1007/s00445-012-0635-8.
Vergniolle, S., Ripepe, M., 2008. From strombolian explosions to fire fountains at Etna volcano (Italy): what do we learn from acoustic measurements?. Geol. Soc. Lond. Spl. Publ. 307, 103–124.
Wilson, L., 1972. Explosive volcanic eruptions-II the atmospheric trajectories of pyroclasts. Geophys. J. R. Astron. Soc. 30, 381–392.
Wright, H.M.N., Cashman, K.V., Rosi, M., Cioni, R., 2007. Breadcrust bombs as indicators of vulcanian eruption dynamics at Guagua Pichincha volcano, Ecuador. Bull. Volcanol. 69, 281–300.